Engineering Structures 292 (2023) 116559

Contents lists available at ScienceDirect

Engineering Structures

journal homepage: www.elsevier.com/locate/engstruct

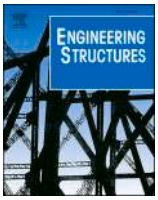

Experimental tests and numerical simulations on the mechanical response of RC slabs externally strengthened by passive and prestressed FRP strips

Niloufar Moshiri [a], Enzo Martinelli [a,b], Matteo Breveglieri [a,*], Christoph Czaderski [a]

[a] Empa, Swiss Federal Laboratories for Materials Science and Technology, Ueberlandstrasse 129, Dübendorf, Switzerland
[b] Department of Civil Engineering, University of Salerno, Via Giovanni Paolo II 132, 84084 Fisciano, Italy

ARTICLE INFO

Keywords:
Concrete
Prestressed FRP
Numerical modeling
Externally Bonded Reinforcement of Groove (EBROG)
End Anchorage

ABSTRACT

Externally Bonded Reinforcement on Groove (EBROG) method has been introduced to enhance the bond resistance of FRP strips to concrete. It has demonstrated that EBROG generally outperforms EBR in terms of load-transfer capacity between FRP strips and concrete. The present study aims to further demonstrate the potential of EBROG applied for flexural strengthening. A specimen reinforced according to the EBR solution and a nominally equal one reinforced through the EBROG system are first presented. Then, the performance of a newly fully-composite mechanical end anchorage for prestressed FRP strip to be used in conjunction with the EBROG method is investigated. The experimental results show that the premature debonding observed in EBR is avoided by EBROG in the case of "passive" FRP strips. Moreover, the combination of EBROG and end anchorage demonstrates their effectiveness, as the pre-stressed slab exhibits the full exploitation of the FRP up to rupture. Numerical analyses, carried out by means of a model already presented by the authors, show that the structural response of the tested slabs can be simulated in a very accurate manner if consistent assumptions are made in terms of bond-slip laws adopted to describe the interaction between FRP and concrete in EBR and EBROG.

1. Introduction

During the last three decades after the first pioneer applications [1], Fiber-Reinforced Polymer (FRP) systems have gained consensus among the technical solutions possibly available for enhancing the structural performance of existing RC members either affected by degradation effects [2] or subjected to an increase in the expected actions [3]. Specifically, externally Bonded Reinforcement (EBR) is the most common technique for bonding FRP fabrics or strips to concrete members [4]. This has certainly the advantage of being lightweight and of rapid application, but it is also characterized by some drawbacks [5]. One of the main weaknesses exhibited by FRP EBR of RC beams is the premature occurrence of the so-called debonding failure, which can develop in different ways [6] generally classified as either plate-end or intermediate debonding failure [7]. The latter is driven by several physical quantities and parameters [8], whose influence is investigated in numerous studies [9–11], to shed a final and clarifying light on this phenomenon. A further complication is that interfacial defects and concrete heterogeneity will affect the bond performance between FRP and concrete [12,13].

The possibility to avoid the occurrence of FRP debonding or, at least, to constrain its unconstrained development was pursued, at the end of the 2010s, by figuring out and introducing "mechanically fastened" FRP systems [14]. However, they soon showed their limitations with respect to the EBR FRP in terms of interaction effectiveness with the RC member [15]. An effective alternative is the so-called near-surface mounted (NSM) reinforcement, in which FRP is bonded into grooves filled with adhesive [16,17]. Nevertheless, to avoid damaging the existing internal steel, this method can only be applied in cross-sections with a reasonable thickness of the concrete cover. A more convincing and robust technical solution emerged when the so-called Externally Bonded Reinforcement On Grove (EBROG) solution was developed to enhance the bond strength between FRP strips and concrete substrate [18,19]. Specifically, the method is based on realizing grooves throughout the concrete substrate where the FRP strip is supposed to be placed. Those grooves are then filled with epoxy resin and the FRP strip is bonded through it, which significantly increased the potential fracture surface and, then, the resulting strength of EBROG FRP connections, with respect to the "traditional" EBR solutions [20].

The improved EBROG bond strength in comparison to the EBR was proved through lap-shear bonded joints tests as well as through bending tests on RC elements using both CFRP strips and fabrics, regardless of the

* Corresponding author.

https://doi.org/10.1016/j.engstruct.2023.116559
Received 19 February 2023; Received in revised form 30 May 2023; Accepted 30 June 2023
Available online 10 July 2023

number of grooves or their geometry [21]. In a lap shear test, the EBROG bonded CFRP plates can approximately carry twice as much force as the EBR method. It has also been demonstrated that the larger grooves are the higher the bond strength and the depth of the groove has a greater effect than the width [21]. The observed failure was no longer owing to debonding in the thin concrete layer right below the adhesive as typically occurs in the EBR, but in a cohesive failure in the adhesive [22] or deeper failure in adhesive and concrete [23,24]. Studies on the local-bond slip behavior have highlighted a lower initial elastic stiffness and a strong increase in the value of the fracture energy compared to EBR. Additionally, a longer effective bond length was observed due to the higher interfacial slips [22]. The EBROG method with "passive" (or "non-prestressed") FRP strips can significantly increase the ultimate load-carrying capacity of concrete members, higher strain in the strengthening can be achieved in comparison to the EBR, by enabling a fracture surface to develop deep in the concrete below the grooves [25]. As a result, the properties of the composite material are better exploited, as both intermediate debonding and anchorage failures can be delayed, up to the tensile failure of CFRP [26].

Nevertheless, the greatest advantage in the use of the EBROG method emerges especially in the case of prestressed CFRP strips [27]. In such systems, the CFRP prestressing force is typically transferred from the end of the laminate to the concrete substrate over a short length [28]. In EBR systems, this is possible only by adopting either mechanical anchorage or special techniques like the so-called "gradient anchorage method" [32,33]. It must be pointed out that, unlike during the lap-shear test, in which interlaminar shear forces are dominating, during the release phase, a considerable force component normal to the surface of the strips take effect. Normal and shear stresses lead to a mixed shear/peeling failure if the bond strength is too weak to transfer the stresses deep into the concrete substrate, as occurs with the EBR method.

The improved bond strength in the EBROG method originates from the fact that during prestress force release, instead of shear/peeling failure in a thin layer of concrete, a deep fracture surface is mobilized in the concrete [29]. Therefore, in the EBROG method, a moderate prestressing force can be anchored without any additional end anchorage. In order to prestress the CFRP to higher forces, which are often required in practical strengthening applications, an additional anchoring system based on the EBROG method and U-shape CFRP stirrups was developed and its effectiveness is demonstrated hereafter in this work [30]. The U stirrup works as a staple, the two legs are glued in holes drilled into the concrete and the crown restraints the uplift of the strips by controlling the normal force during releasing.

Compared to the Near Surface Mounted (NSM) method, which also entails a high bond capacity, the EBROG method is significantly less invasive, as the depth of the grooves to be cut in the concrete cover is smaller than with NSM [30]. Another substantial advantage lies in the greater ease of prestressing operations. NSM strips have the advantage of not requiring a special end anchorage; however, their application on the construction site can be complex, as additional space for the CFRP prestressing anchoring system at the end of the grooves must be provided.

This paper aims at demonstrating the advantages of the EBROG technique with respect to the classical EBR one and to show the functionality of the newly developed end anchorage method. To this aim, it reports the experimental results of three RC slabs, 6 m in length, externally strengthened by a FRP strip connected to the RC soffit according to either of the aforementioned technical solutions. Besides the two cases of two RC slabs with "passive" FRP strips, a further RC slab strengthened by a "prestressed" EBROG FRP is also considered: in this case, an all-FRP stirrups end-anchorage is applied with the aim to restrain the imposed prestressing action to the composite strip. The comparison among the relevant results for the three tested RC slabs points out their different mechanical responses. Some numerical analyses were carried out by utilizing a mechanical model, derived from a slight extension of a previous one already formulated by the authors [32,34,35,36] and implemented in Matlab [37]. This led to an in-depth interpretation and understanding of the inherently different responses controlled, on the one hand, by the different bond-slip interactions that characterize EBR and EBROG, and, on the other hand, by the effect of prestressing.

Table 1
Test program.

Label	Strengthening method	Pre-strain	Prestressing ratio	Prestressing force *Fp*	Concrete cubic comp. strength
				[kN]	[MPa][a]
EBR	EBR	–	–	–	47. 6
EBROG	EBROG	–	–	–	40. 4
EBROG-P	EBROG	0.6%	36%	140	*[b]

[a] Tested according to EN 12390–3:2009.
[b] No test data was available.

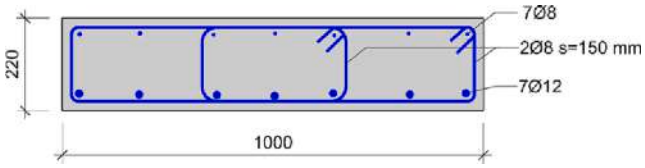

Fig. 1. Slab cross-section and details of the internal steel reinforcement, concrete cover: 25 mm (all dimensions in mm).

2. Materials and methods

2.1. Constituting materials and specimens preparation

Three reinforced concrete slabs strip with a total length of 6500 mm and a cross-section of 1000 mm × 220 mm (width × height) were strengthened using different solutions based on bonded CFRP strips. The slabs were cast on three different days with concrete mixtures of equal characteristics (maximum aggregate size of 32 mm, cement content 300 kg/m3). The concrete compressive strength exceeded a cubic compressive strength of 40 MPa as reported in Table 1. The slab longitudinal reinforcement consisted of seven 8 mm-diameter bars at the top and seven 12 mm-diameter bars at the bottom (Fig. 1). Stirrups of diameter 8 mm with 150 spacing were used as transversal reinforcement. The clear concrete cover was set to 25 mm.

Unidirectional CFRP strips with width of 100 mm, thickness of 1.4 mm, ultimate tensile strength higher than 2800 MPa, and fiber volume fraction larger than 68%, according to the manufacturer, were used in strengthening the slabs [38]. The elastic modulus of 168 GPa was measured in the laboratory, therefore the tensile rupture strain was estimated to be equal to 16600 microstrain (μm/m).

The adhesive was a two-component epoxy adhesive (S&P 220HP), having an ultimate tensile strength larger than 15.0 MPa and tensile elastic modulus larger than 7.1 GPa, according to the manufacturer test specification [39].

The test program included three large-scale slabs, as is summarized in Table 1. All the slabs were strengthened with one CFRP strip. The first specimen, labeled as "EBR", was strengthened with a passive (non-prestressed) CFRP strip using the conventional EBR method. The concrete surface was ground with a portable disc grinder before bonding the strip to the slab. Then, the strip was glued to the slab in an overhead position. The second specimen, labeled as "EBROG", was strengthened with a passive CFRP strip using the EBROG method. In this method grooves parallel to the slab's length, are cut in the concrete cover, and filled with epoxy adhesive, then the strip is attached on top of the grooved area

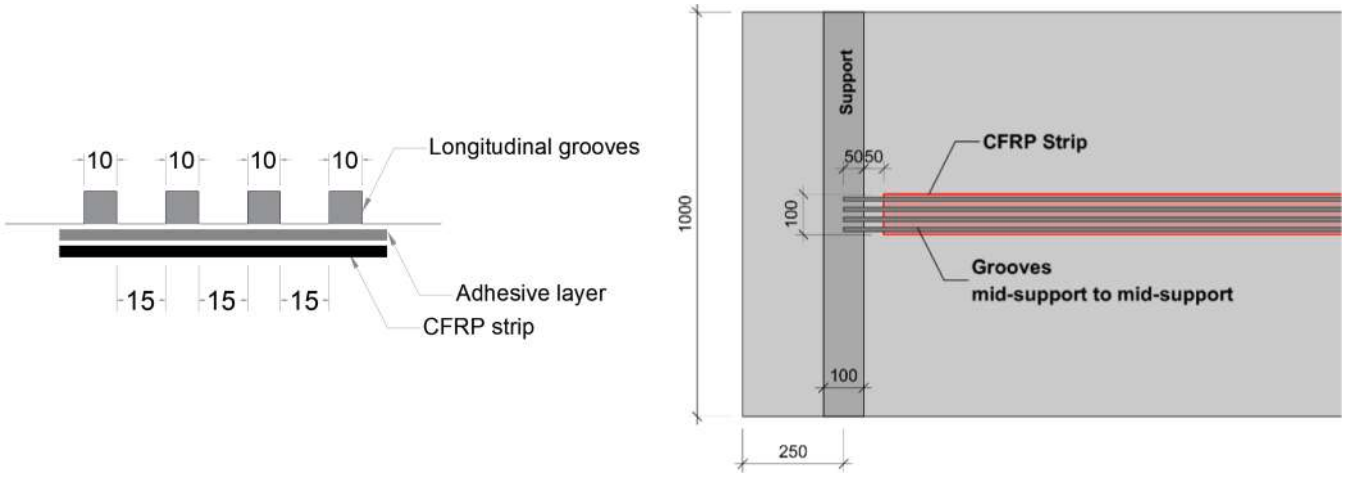

Fig. 2. Details of the EBROG method: (a) Grooves' cross-section, (b) Bottom side of slab end strengthened with EBROG method.

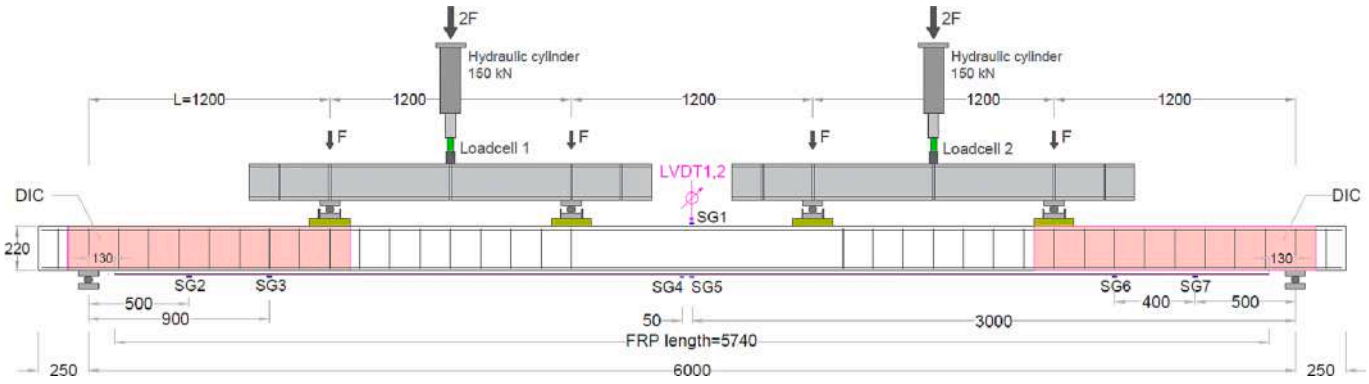

Fig. 3. Schematic drawing of the test setup.

with the same epoxy adhesive. In the tested specimens four grooves of 10 mm × 10 mm with clear distance of 15 mm from each other were cut over a length of 6000 mm (Fig. 2). The last specimen, labeled as "EBROG-P", was strengthened with a prestressed CFRP strip using the EBROG method. The strengthening procedure followed an identical grooving preparation work as for the second specimen, in addition after filling the grooves with adhesive, the strip was glued on top of the grooves and prestressed to 140 kN, which corresponds to a pre-strain of 0.6% and stress of 1000 MPa. To anchor the prestressing force, a newly developed end anchorage system using the EBROG method and U stirrups was utilized. More details on the end anchorage system and the prestressing procedure are presented in section 2.4. Novel end anchorage system. Before cutting out the grooves, the bonding area of the two slabs strengthen according to the EBROG method has been ground similar to the conventional EBR specimen. Due to technical difficulties in cutting the grooves and gluing in an overhead position, the strengthening with the EBROG method was carried out on the lab floor with the working side facing up.

The two non-prestressed slabs were tested approximately one month after being strengthened, meanwhile, for the prestressed slab, the test was carried out 13 days after the strengthening operations.

2.2. Testing procedure and measurement equipment

Slabs were tested under 6-point bending loading as displayed in Fig. 3. The load was applied through two hydraulic cylinders, each having a capacity of 150 kN, which transferred the force to the slab through steel I profiles. The test was performed in displacement control mode at a speed of 12 mm/min and the applied forces were measured with two 150 kN-load cells. The adopted loading protocol is displayed in Fig. 4, which denotes three cycles for each load step of 20, 60, and 100 kN. After completing all the cycles, the displacement was increased up to the failure of the slab. A further unloading cycle shortly before the final

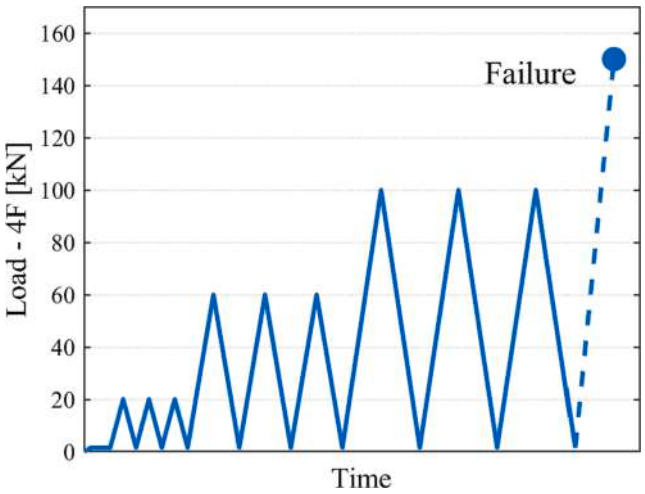

Fig. 4. Load protocol.

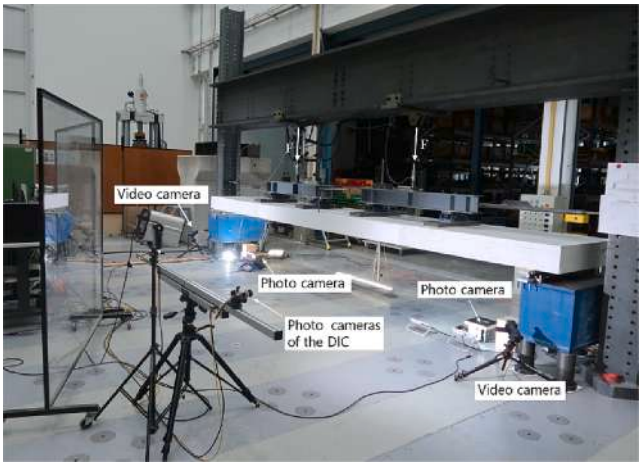

Fig. 5. Photo of the test setup.

failure was necessary for slab EBROG as the maximum stroke of the loading cylinders was reached.

Mid-span displacement of the slab was measured with two 200 mm transducers mounted on the top side of the slab one (LVDT No.1 and No.2 in Fig. 3). Concrete compression strain in the middle of the slab was measured with one strain gauge of type 100/120 LY41(HBM-HBK GmbH). In addition, six strain gauges of type 6/120 LY66 (HBM-HBK GmbH) were used to measure the strain in the CFRP strip at six different locations (Fig. 3). One pair of strain gauges were glued in the middle of the strip, to monitor the maximum CFRP tensile strain, meanwhile the other two pairs were glued at the end of the anchorage zone and approximately below the force point application mainly to provide information on the anchorage and possible strain drops in the prestressed slabs.

Two video cameras and two DSLR cameras were placed near the slab end to observe the debonding mechanism during the failure test. Test instrumentation and measurement system are displayed in Fig. 5.

2.3. DIC measurement

To measure the three-dimensional deformations and record the crack pattern at slab ends, two-digital image correlation (DIC) systems were used (Fig. 5). Each system comprised two 12 megapixels digital cameras, placed 1180 mm far from each other on a frame, and 2200 mm far from the slab's surface. The adapted measuring setup leads to a measurement field length of 1300 mm, as shown in (Fig. 3). A random high-contrast speckle pattern was applied on the slab surface by using a black roller on the pre-painted white surface of the slabs. The displacements field was processed using the VIC3D software from the company Correlated Solution Inc. [40]. In-plane and out-of-plane deformations, as well as the principal strains, which were used to demonstrate the cracks on a concrete surface, were determined accordingly.

2.4. Novel end anchorage system

To anchor the prestressed CFRP strip in EBROG-P, a new anchorage system was developed. This is an adaptation of the end anchorage system commercialized by S&P Clever Reinforcement Company. The S&P system uses metallic bolts and plates at the strip end for permanent fastening. The newly developed technology, made use of the existing prestressing claps and frames, though the fixing-metallic plates were replaced by a full-composite system based on the EBROG method and special CFRP-U stirrups. This system was developed through an extensive study at Empa [30], during which a large experimental campaign was followed to investigate the ultimate capacity of the system as well as its performance in service conditions [31]. The current work presents only the definitive solution; therefore, specific details on the optimization of the anchorage system are here omitted.

The end anchorage system is presented in Fig. 6. First, the longitudinal grooves as well as the holes for the stirrups legs were made, and the prestressing system (frames and claps) was mounted. Then, the grooves were filled with epoxy adhesive and, a layer of adhesive was applied to the top of the CFRP strip. The strip was mounted over the filled grooves and later pulled from one end by a hydraulic cylinder (Fig. 6b). Fig. 6c shows the placement of the four U stirrups inside the holes as well over the prestressed CFRP strip. A layer of adhesive was applied between stirrups and laminates and a Teflon plate was installed inside the prestressing frame to hold the U-stirrups in position during the curing period (Fig. 6 d).

The metallic clamps and frames keep the prestressing force constant for two days, which is the time needed by the adhesive to harden, after this period all the clamps and frames were removed. The final configuration of the strengthening solution comprised of a prestressed CFRP strip and the U stirrups is depicted in Fig. 6 e. It is worth mentioning that the bolts, visible in Fig. 6 e, are not needed anymore and can be cut afterward. As a result, the final volume occupied by the proposed method is minimal. Fig. 6 f and Fig. 6 g present the geometry of the novel anchorage system and the U stirrups.

During the strengthening of Slab EBROG-P, the strain in CFRP strip was monitored at six different locations (Fig. 3). Strain gauges No. 2 and 7 were glued at a distance of 400 mm from each strip end, strain gauges No. 3 and 6 at a distance of 800 mm from each strip end, strain gauge No. 5 in the middle of the strip, and strain gauge No. 4 with a distance of 50 mm from strain gauge No. 5. The measured strains of the six strain gauges are plotted in Fig. 7 for the working stages: prestressing, curing of the adhesive and releasing of the force at the strip ends. After fixing the clamps and the removal of the hydraulic cylinder, all the strain gauges experienced a decrease in the strain due to elastic deformations and reached approximately 5900 μm/m. After two days (curing time), the adhesive achieves sufficient strength and the prestressing system was removed resulting in a slight reduction of strain at two strip ends. Strain gauges No. 2 and 7 lost about 50 μm/m and reached 5730 and 5670 μm/m. During the release of the force at the strip ends, small cracking occurred at the end of the bonded area. More details on the mechanism of releasing step can be found in [30]. No meaningful strain changes were observed at the location of the other four strain gauges. Between day 2 and day 6 a negligible prestressing loss could be observed in the strain gauges closer to the anchorage zones. When the slab was turned and installed in the testing setup, the strains slightly increased due to its self weight. Afterward, from day six until day 13, the strain in the strip increased to some extent due to concrete creep in the compression top side of the slab. The maximum strain in the middle of the strip was around 5950 μm/m before starting the bending test. This value was considered in the finite element modeling presented in Section 4. Temperature changes could be disregarded because all the operations were carried out in the lab, where the temperature does not deviate significantly from 20 °C.

3. Experimental results

3.1. Overall behavior

A six-point loading test was performed until complete failure of the slabs. An overview of the test results is presented in Table 2. In this table, maximum load, which is the total force applied on the slab (4F), and maximum deflection (D_{max}), concrete compression strain (ε_c), and strip strain (ε_{FRP}) corresponding to the ultimate load are reported. The Δ values represent the increment of the recorded measurands in comparison the EBR slab.

The maximum load capacity of EBR slab was 100.5 kN. The slabs strengthened with non-prestressed and prestressed EBROG methods experienced 135.9 and 132.5 kN load capacity, indicating more than

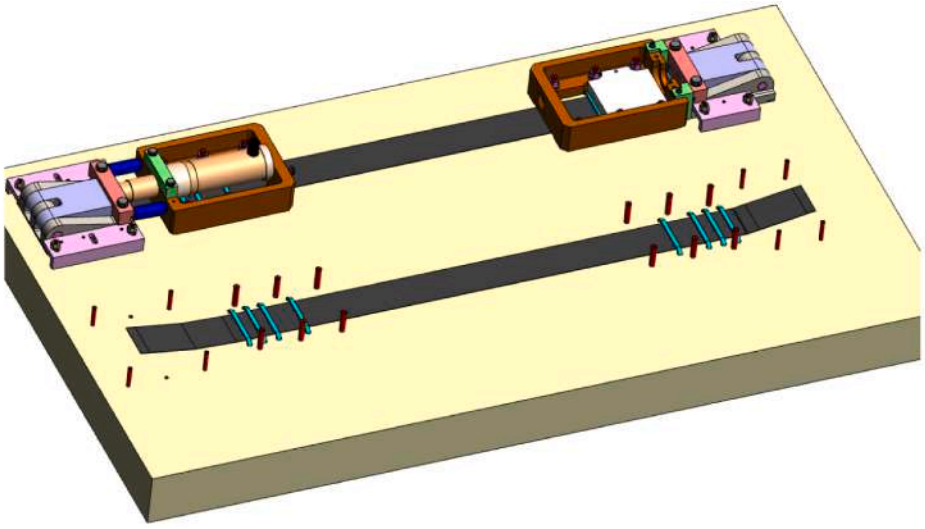

(a) Schematic view of the developed end anchorage system *

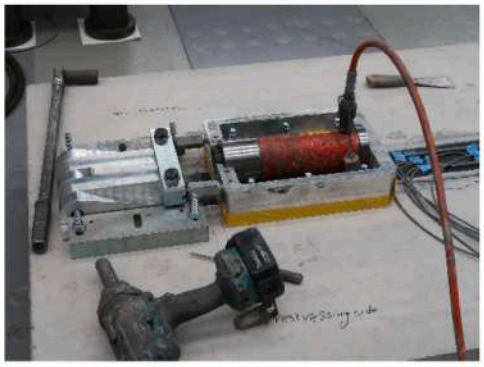

(b) Attaching the strip, fixing the frame, and prestressing it up to desired pre-strain level

(c) Installing U stirrups over the prestressed strip

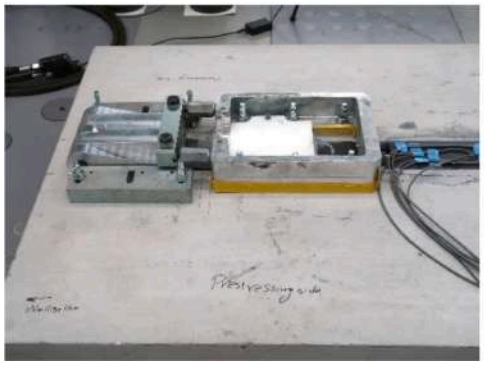

(d) Installing a Teflon plate over U stirrups to keep them in the right position during curing

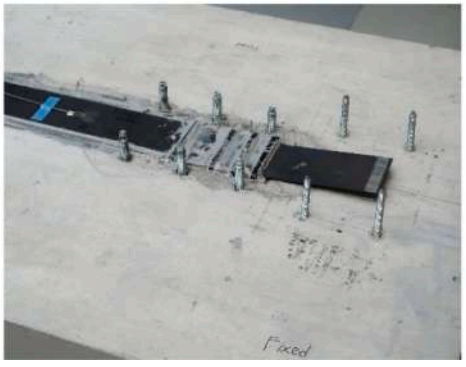

(e) Removing the frames and clamps after curing

Fig. 6. Novel end-anchorage system for prestressed CFRP strip (* Image provided by S&P Clever Reinforcement Company AG, Switzerland).

30% increase in the maximum capacity compared to the slab strengthened with EBR method. In addition, the maximum strains of the CFRP strip in EBROG and EBROG-P slabs were 12900 and 12700 μm/m representing almost 70% increase compared to 7500 μm/m in EBR slab strip. This shows a significant increase in the CFRP strain, which entail a more efficient use of the FRP material through the EBROG method.

It is believed that the CFRP strips, in both EBROG strengthened slabs, reached their ultimate tensile capacity, meanwhile, the EBR slabs failed due to premature debonding.

Photos and videos, as further discussed in Section 3.2., prove the tensile rupture of the strip in EBROG and EBROG-P slabs, without showing any sign of end-anchorage failure. Therefore, from the comparable maximum deformation achieved in both CFRP strips bonded according to the EBROG method, it appears that the maximum measured

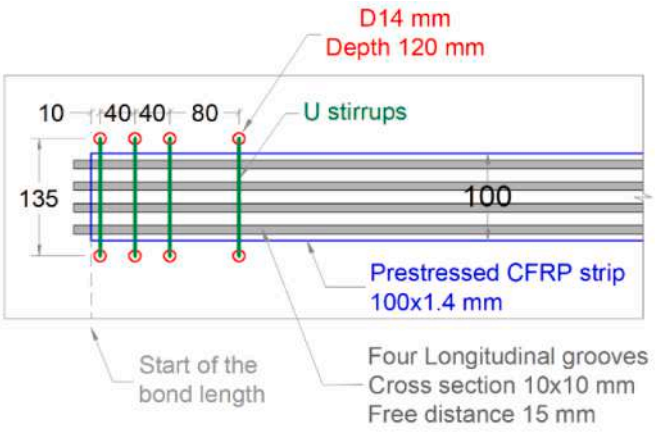

(f) Position of U stirrups at the strip end

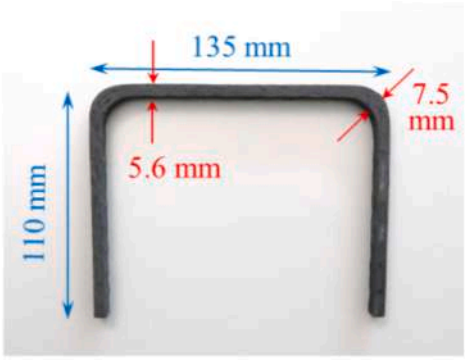

(g) Dimensions of the U stirrup

Fig. 6. (*continued*).

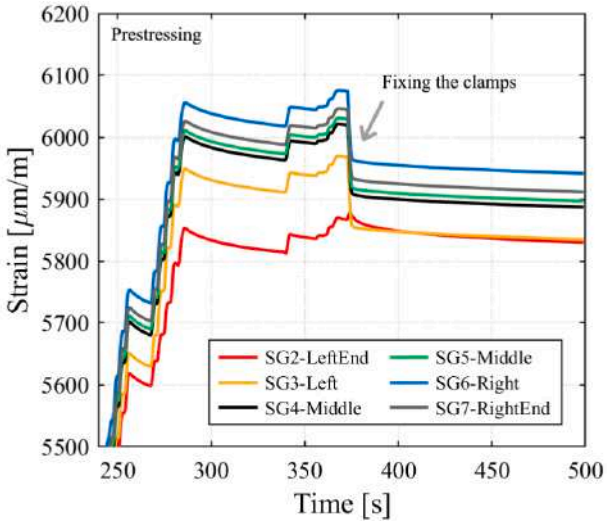

(a)

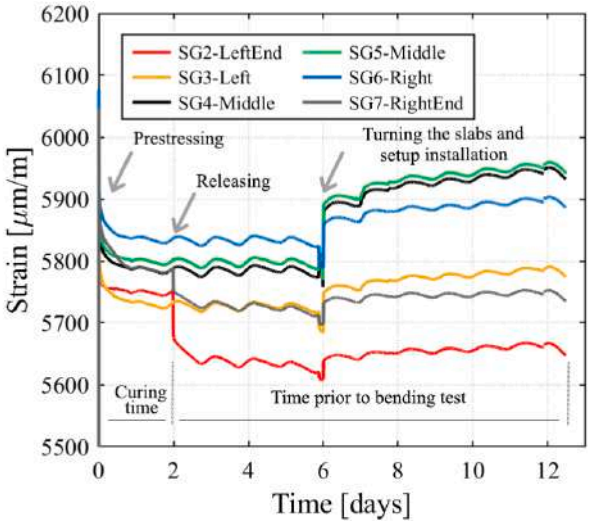

(b)

Fig. 7. Monitoring of strains in the EBROG-P: (a) Prestressing operation, (b) Prestressing, curing, releasing (removing the clamps and frames) phases before the running of the bending test.

Table 2
Test results.

Slab	$4F$	$\Delta - 4F$	D_{max}	$\Delta - D_{max}$	ε_c	Δ -ε_c	ε_{FRP}	Δ - ε_{FRP}
	[kN]	[%]	[mm]	[%]	[μm/m]	[%]	[μm/m]	[%]
EBR	100.5	–	127.8	–	−1450	–	7500	–
EBROG	135.9	35%	216.9	70%	−2300	59%	12,900	70%
EBROG-P	132.5	32%	130.1	2%	−1560	8%	12,700	69%

strain can be assumed as an approximation of the rupture strain for CFRP strips for the presented testing configuration. It was already mentioned that the ultimate tensile rupture of the strip, reported by the manufacturer and determined through tensile coupon tests, was 16600 μm/m. The tensile stresses in the CFRP strip when attached to a tensile face of a slab are not uniform in the whole width, in contrast to coupon tests. Not only the strip on a slab suffers from local stress concentration due to surface irregularities (see Fig. 11), but also is not completely straight as follows the curvature corresponding to the slab deflection. These all may affect the rupture strain of the CFRP strip and reduce it compared to a pure tensile coupon test.

In the prestressed slab, despite the initial pre-strain, the interfacial shear stresses at the slab interface can be assumed to be zero, (except for the end anchorages) if no external load is applied. Interfacial stress generates, as in the case of passive strips, only upon the external load application. Therefore, it can be concluded that at the same CFRP strain level, the shear stresses in EBROG-P slab are lower compared to those in EBROG slab. As a result, in the prestressed slab, if the ultimate deformation of the composite material had not been reached, the slabs would have been able to undergo a higher ultimate load-carrying capacity.

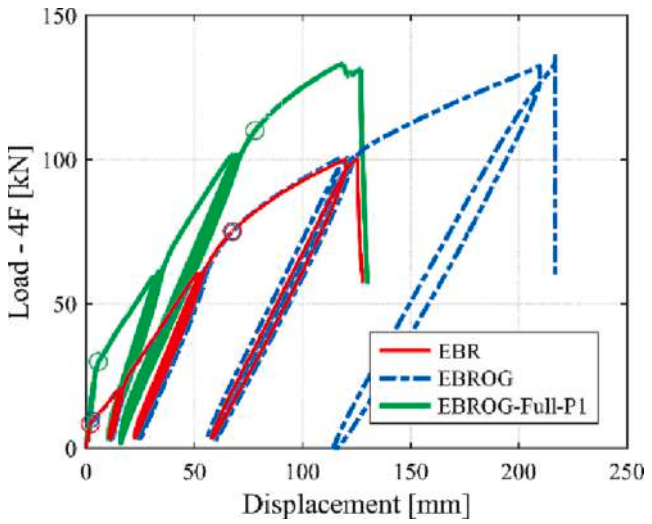

Fig. 8. Load–deflection behavior, the markers indicate the cracking and yielding points.

Fig. 8 presents the Load – deflection behavior of three slabs up to failure. The plots of EBR and EBROG slabs are completely superimposable until the EBR strip, debonds at 100.5 kN. The cracking and yielding points of these two slabs were approximately 10 kN and 75 kN, respectively. The prestressing of the CFRP strip in EBROG-P slab increased the cracking and yield load to almost 30 kN and 110 kN, indicating a significant improvement compared to that of the non-prestressed slab. In addition, the deflection of EBROG-P slab was considerably smaller than that of the other two slabs at similar load levels. The application of prestressed CFRP strip through EBROG method and the novel full-composite end-anchorage, can therefore substantially improve the serviceability limit state, still allowing the yielding of the internal reinforcement and without crucially reducing the slab deflection at failure.

In addition, it can be observed that the maximum deflection of EBROG slab was 70% higher compared to EBR slab. Therefore, for strengthening applications in which the serviceability limit state is not critical, the passive EBROG method is an excellent solution to increase the load-carrying capacity without reducing the deflection capacity at ultimate limit state as it occurs in the EBR technique.

Load–strain behavior of the tested slabs is illustrated in Fig. 9. The positive and negative trajectories depict the CFRP deformation in the middle of the slabs (SG5), and in the concrete (SG1), respectively. The two strain gauges installed in the middle of the strip had approximately similar values. EBR and EBROG slabs demonstrated similar performance in terms of load–strain trajectories up to the EBR strip debonding. As already observed in Table 1 the EBROG method, owing to higher bond resistance between strip and concrete surface, was able to avoid the debonding, therefore significantly higher strain in the CFRP strip was achieved. The CFRP strain in the strip of the EBROG-P slab started from the prestressing value of 5950 μm/m and increase up to 12700 μm/m.

The strain gauges on the EBR strip at 800 and 400 mm from the strip end measured a maximum strain of 2249 and 880 μm/m, vs the 3034 and 1276 μm/m in the EBROG strip. The higher strain is related to the higher slab's load-carrying capacity. In both specimens the strains measured close to the support, i.e. near the beginning of the cracked zone, were far below the debonding strain which can be experienced in typical EBR or EBROG end anchorage.

In the prestressed slab the strain gauge at 400 mm exhibits a negligible increase of strain, which is in agreement with the crack pattern presented in Fig. 13, in which no cracks close to the end anchorage zone are visible.

The strain in the strain gauges at 800 m from the strip end in EBROG-P is 7600 μm/m, therefore the increase due to external loading is approximately 1750 μm/m.

The graphical representation of force-strain trajectories at 400 mm and 800 mm end are omitted; their values are used for selected load step, as model validation in the numerical section (Figs. 22-24).

The maximum concrete compression strain reached 2300 μm/m in EBROG slab, showing 59% increase compared to that of EBR slab, allowing a larger cross-section rotation. The concrete compression strain was still well below the nominal value of concrete crushing strain.

It is worth mentioning that the strain gauge on the concrete compression face of EBROG-P slab was installed after the strip was prestressed. Therefore, the strain gauge reading did not include the effect of prestressing and it started from zero in the load–strain diagram (Fig. 9). This implies that the real compressive stresses were lower than the one shown in the figure.

3.2. Failure mode

Photos of the EBR, EBROG and EBROG-P slabs after failure are presented in Fig. 10, Fig. 11, and Fig. 12, respectively. The videos capturing the failure of the slabs can be found in the **supplementary material** section. It can be observed in Fig. 10 (a) that the failure mode in the EBR specimen was debonding of the CFRP strip from the concrete substrate. A concrete layer was attached to the strip after failure, showing that debonding fully occurred inside the concrete. In addition, by inspecting the videos it was observed that the debonding happened approximately in the middle of the slab strip. Therefore, it is possible to assume that the

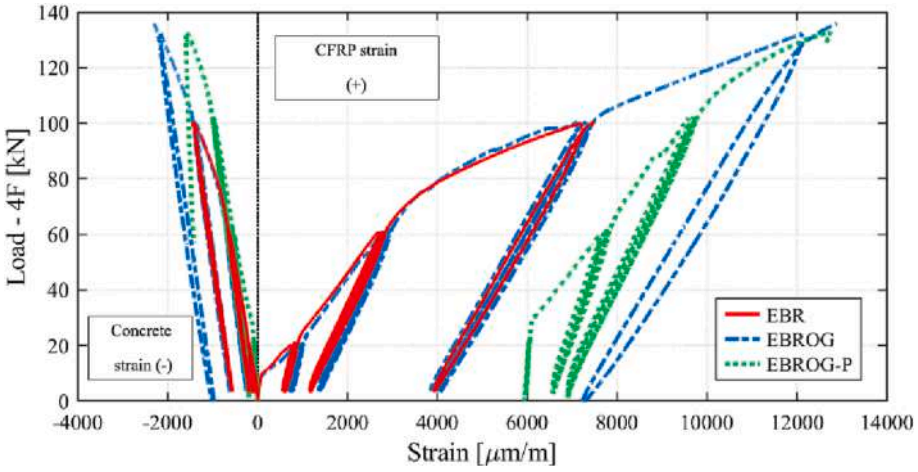

Fig. 9. Load–strain behavior comparison.

Fig. 10. Failure mode of EBR slab.

Fig. 11. Failure mode of EBROG slab.

dominant failure mode in the EBR slab was intermediate debonding.

On the other hand, the governing failure mode in the EBROG slab was assumed to be the rupture of the CFRP strip, as depicted in the left photo of Fig. 11. At ultimate stage, the strip ruptured at a distance of approximately 1770 mm from support. Deep cracks occurred in the concrete substrate due to high interfacial stresses transferred from the strip into the concrete, Fig. 10 (b). A very thin layer of the CFRP fibers was visible after failure on the detached surface, pointing out inter-laminar cohesive failure inside the CFRP layer, which probably was triggered only at CFRP strains near rupture.

Failure of the EBROG-P slab included rupture of prestressed CFRP strip, deep cracks inside concrete below the grooves, and debonding of the strip from concrete substrate. Nevertheless, the dominant failure mode was CFRP rupture, at a distance of approximately 2000 mm from support. Photos of the end anchorage zones in Fig. 12(b) confirm no major failure in the anchorages. The CFRP strip slipped out of the end anchorage on the prestressing side (see bottom left photo in Fig. 12(b), presumably after failure of the slab and rupture of the strip. The video

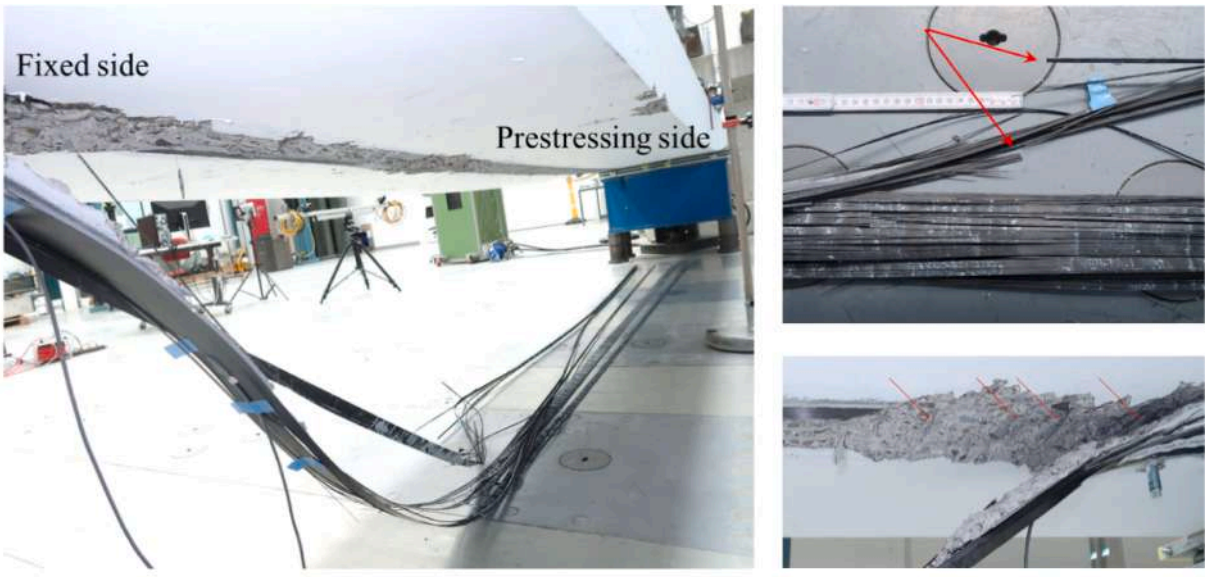

(a)

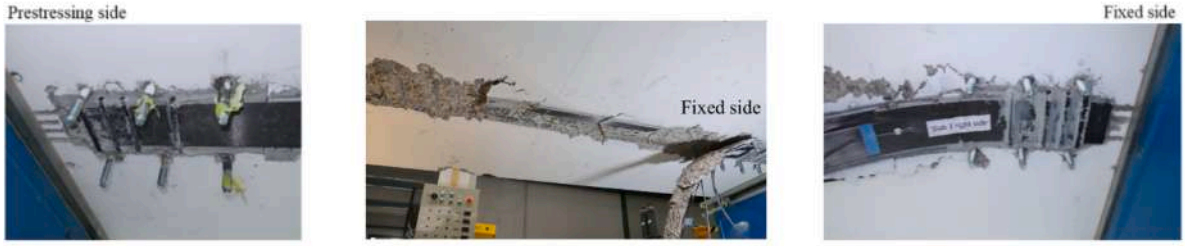

(b)

Fig. 12. Failure mode of prestressed slab (EBROG-P): (a) strip failure and cracks in the concrete below the adhesive, (b) end anchorage failure.

recordings showed the rupture of some fibers during the final stages of the test in EBROG and EBROG-P.

3.3. Cracks

The crack pattern, processed from the left DIC measurement field, is displayed in Fig. 13(a); the represented load of 80 kN slightly exceeds the yield load for the non-prestressed slabs. Support and load application point are marked in the images. Six cracks can be observed in the shear span of EBR and EBROG slab, meanwhile as expected for the prestressed element a lower number of cracks (three) is visible in the EBROG-P slab. Total force–crack widths diagrams for the crack at 1200 mm far from the support (i.e., the crack under the load application point) are plotted in Fig. 13(b). It is perceived that the crack width for EBROG slab was slightly lower than that of EBR slab. However, the crack width in the prestressed EBROG-P slab was considerably smaller at all load levels, compared to the other two non-prestressed slabs. It is concluded that the novel end anchorage system considerably enhanced the serviceability behavior in terms of the number of cracks and crack width, in addition to the cracking load as discussed earlier.

4. Numerical analyses and comparisons

4.1. Outline of the numerical model

The mechanical behavior of the tested RC slabs was further scrutinized by means of numerical simulations, which aim at enriching the empirical observation with a mechanically consistent interpretation. Specifically, the numerical procedure employed for this aim is an extension of the model already proposed in a previous study [34], with the addition of external prestressing in the FRP strip [32]. Moreover, the effects of the possible interface slips between the FRP strip and the concrete substrate were simulated as part of a partial-interaction two-layer composite beam theory [35]. Therefore, the main kinematic assumptions of the present model are listed below:

- the RC slab was modeled as a Timoshenko beam, while the FRP strip was only characterized in terms of axial stiffness;
- the RC slab and the FRP strip may exhibit relative axial displacements (slips), but relative transversal displacements were restrained.

Based on these assumptions, an “exact” 2-node beam-like Finite Element can be derived, which is capable of simulating the linear elastic response of two-layer composite beams in partial interaction like the one under consideration [35]. Fig. 14 depicts a sketch of the element kinematics, which is characterized by 6 degrees of freedom for each element corresponding to the transversal displacement v, the rotation φ and the relative interface slip s at the two element ends i and j. It also depicts a scheme of the discretization (consisting of 30 elements and 31 nodes) of one half beam adopted in the following analyses. It is worth to precise that, in the adopted model, the interface stiffness was set to (numerical) zero in the first element to reproduce the fact that the interaction between RC slab and FRP strip started from node 2. Moreover, in the case of the EBROG-P system, the interface slips at node 2 were set to zero, with the aim to simulate the actual boundary condition embodied by the presence of the U-stirrups (see Section 2).

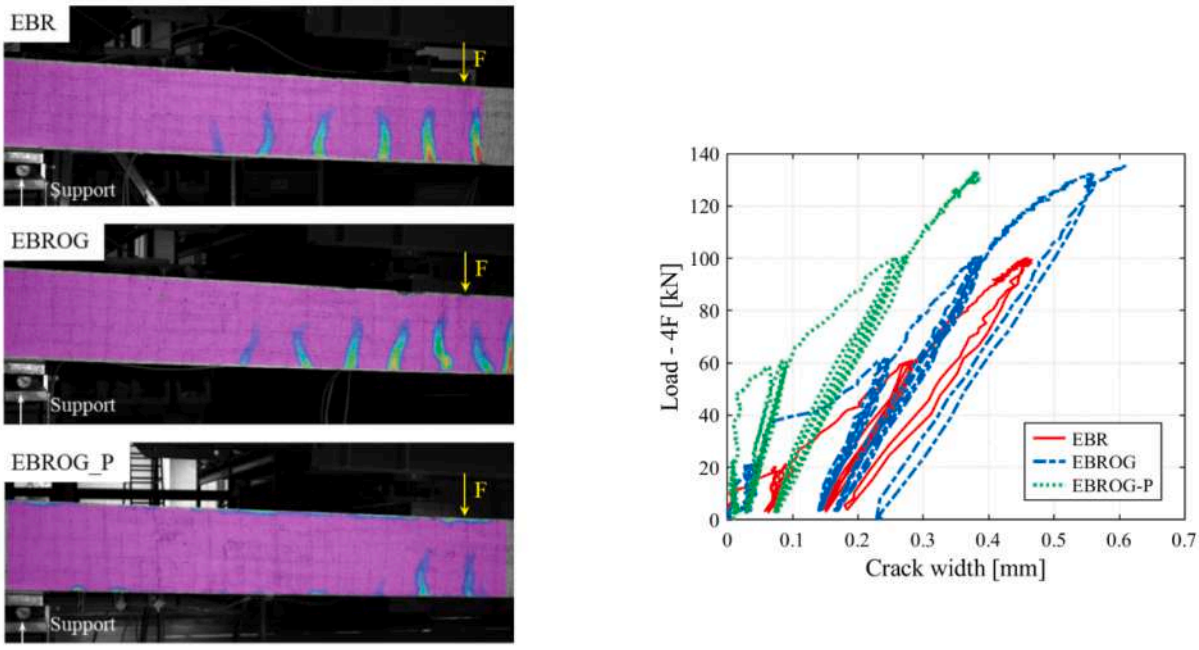

Fig. 13. Crack pattern and crack width: (a) Crack pattern at 80 kN, (b) Load-crack width for the crack at 1200 mm far from the support (i.e., the crack under the first load).

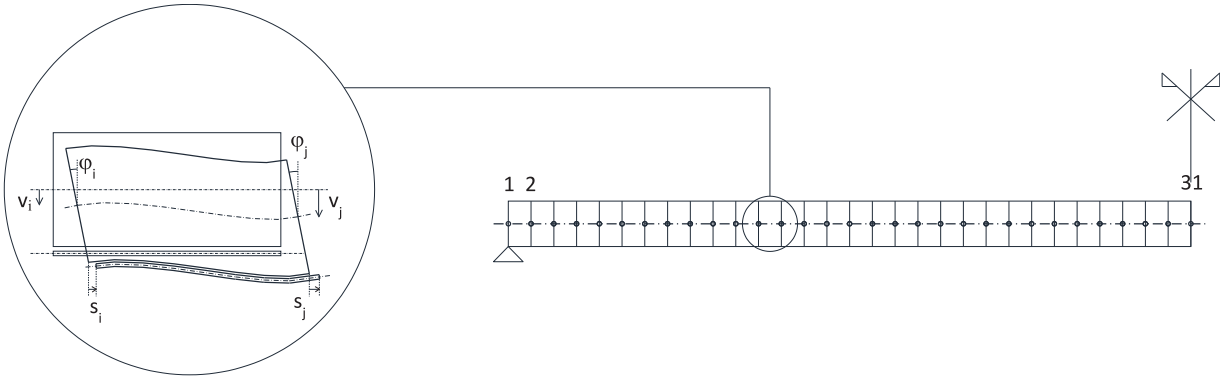

Fig. 14. Finite element kinematic parameters and discretization of the analyzed slabs.

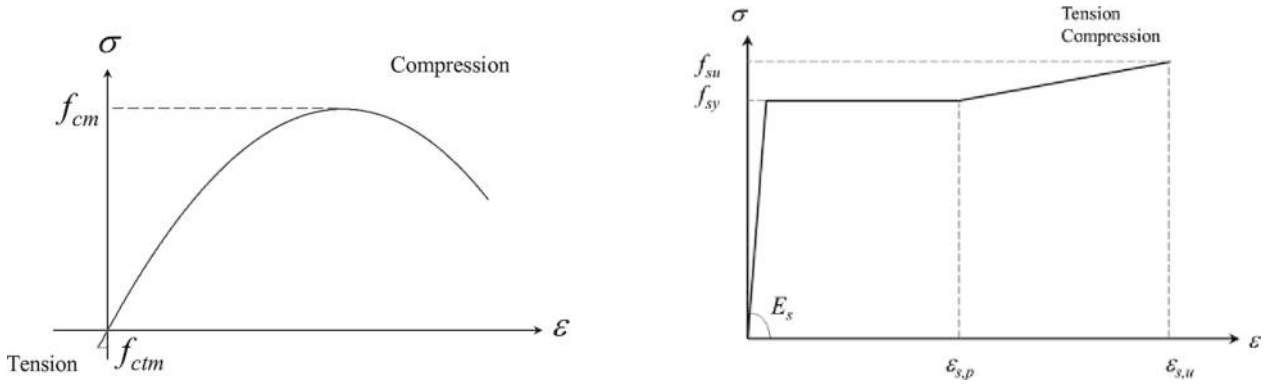

Fig. 15. Stress–strain laws assumed for the concrete and steel.

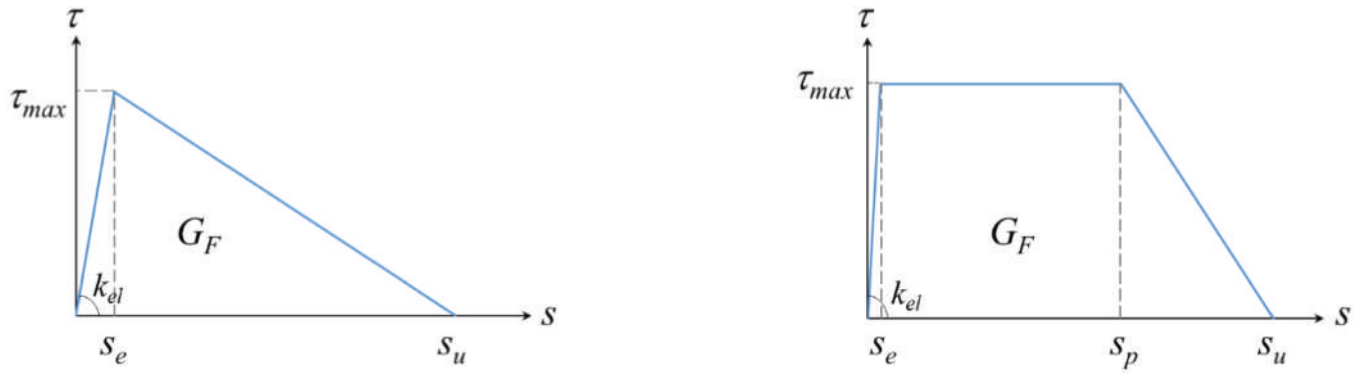

Fig. 16. Bond-slip laws describing FRP-to-concrete interaction for (a) EBR system, (b) EBROG system.

Table 3
Relevant mechanical parameters assumed for the materials.

Slab	Concrete			Steel					FRP		
	f_{cm}[a] [MPa]	f_{ctm}[b] [MPa]	E_{cm}[b] [MPa]	E_s [MPa]	f_{sy} [MPa]	$\varepsilon_{s,p}$ [μm/m]	$f_{s,u}$ [MPa]	$\varepsilon_{s,u}$ [μm/m]	E_f [MPa]	$\varepsilon_{f,u}$ [μm/m]	$\varepsilon_{f,pre}$ [μm/m]
EBR	38.00	2.90	32,837	210,000	550	$3.0x10^4$	640	$6.0\ x10^4$	168,000	$1.4x10^4$	–
EBROG	33.00	2.56	31,476								–
EBROG-P	35.00[c]	2.70	32,036								$5.95x10^3$

[a] Calculated from the cubic strength, using a conversion factor of 0.8.
[b] Estimated from [41]
[c] Estimated value, calculated from the average of the compression tests.

Nonlinear stress–strain relationships were assumed to describe the mechanical behavior of materials and are introduced in the FE model by following a well-known fiber approach and a secant incremental-iterative procedure implemented in a Matlab code [37]. Specifically, as already assumed in a previous work, the concrete in compression is simulated by assuming a Sargin stress–strain law [38] (with a linear-brittle branch in tension), whereas the reinforcing bars are modeled by assuming an elastic–plastic-hardening law. Fig. 15 depicts the typical shape of the aforementioned stress–strain relationship. As for the FRP strip, a simple linear elastic brittle behavior is assumed, which is characterized by given values of Young Modulus E_f and an ultimate strain $\varepsilon_{f,u}$.

The bond-slip laws assumed to simulate the full range response of the FRP-to-concrete interface have different shapes for EBR and EBROG systems. In fact, although the assumption of bi-linear (triangular) bond-slip laws is generally accepted in the literature, recent studies [25] have shown that EBROG systems are characterized by a tougher behavior with respect to similar EBR systems. Therefore, the adoption of a trilinear (trapezoidal) bond-slip law appeared more accurate in simulating the behavior observed both in lap-shear and prestress-release tests of FRP strips glued to concrete through an EBROG solution [29]. Fig. 16 shows the two types of curves and emphasizes the main mechanical quantities that define each of them. A perfect bond was assumed between the internal steel and the concrete (steel–concrete interface) because as already demonstrated by [34] such a model can accurately reproduce the experimental behavior of CFRP-strengthened elements.

Details about the numerical algorithms are omitted for the sake of brevity; however, the present procedure follows the same nonlinear solution approach fully described in a previous paper [34].

4.2. Numerical simulations

The tested slabs can be simulated by assuming a consistent set of values for the mechanical parameters that define the materials and the bond slip law. Table 3 summarizes all the values assumed for the main properties of materials depicted in Fig. 15, namely structural concrete (i.e. mean compressive strength f_{cm}, mean tensile strength f_{ctm}, and Young modulus E_{cm}), rebar steel (i.e. Young modulus E_s, yielding and ultimate stresses, f_{sy} and $f_{s,u}$, respectively, plastic plateau and ultimate axial strains, $\varepsilon_{s,p}$ and $\varepsilon_{s,u}$, respectively), and FRP strip (i.e. Young modulus E_f, ultimate axial strain $\varepsilon_{f,u}$ and possible initially imposed axial strain $\varepsilon_{f,pre}$ for prestressed FRP).

Table 4
Relevant mechanical parameters defining the bond-slip laws.

Slab	k_{el} [N/mm^3]	G_F [N/mm]	s_e [mm]	τ_{max} [MPa]	s_p [mm]	s_u [mm]
EBR	250	0.35	0.025	3.5	–	0.2
EBROG	200	3.19		5.00	0.50	0.80
EBROG-P						

Moreover, Table 4 reports the parameters highlighted in Fig. 16 for the two types of bond-slip laws assumed for EBR and EBROG FRP-to-concrete interface. The parameters listed in the table represent the elastic stiffness (k_{el}), the interfacial fracture energy (G_F), the elastic slip (s_e), the maximum shear stress (τ_{max}), the slip at the end of the plateau phase (s_p), and the ultimate slip (s_u). It is worth highlighting that, for the sake of mechanical consistency, the same bond slip law was assumed for the two EBROG FRP slabs, as it was assumed that the attached materials have the same properties in the two specimens (regardless of the slight difference in f_{cm} assumed for the two slabs and reported in Table 3).

The analyses, run in force control, based on the model in Fig. 14 with the parameters summarized in Table 3 and Table 4, lead to the results reported in Fig. 17. Specifically, it represents the force (4F) vs. displacement (at midspan) relationship for the three tested slab strips. The reference specimen (the slab with no FRP strengthening) was also

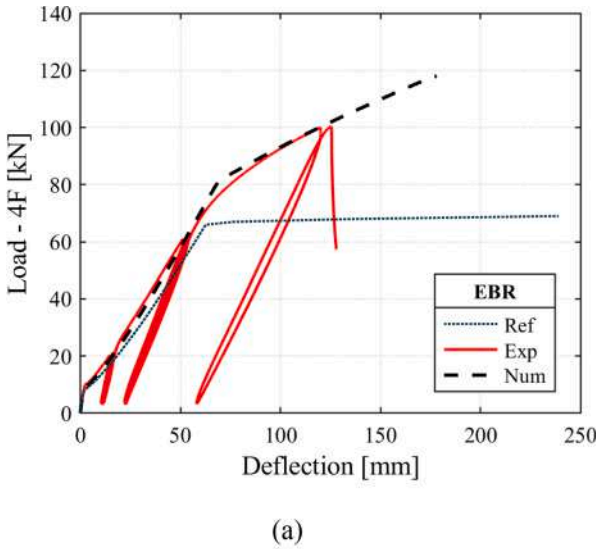

(a)

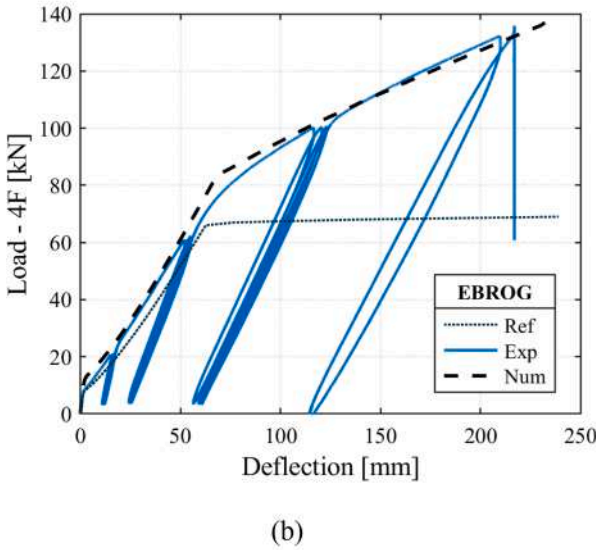

(b)

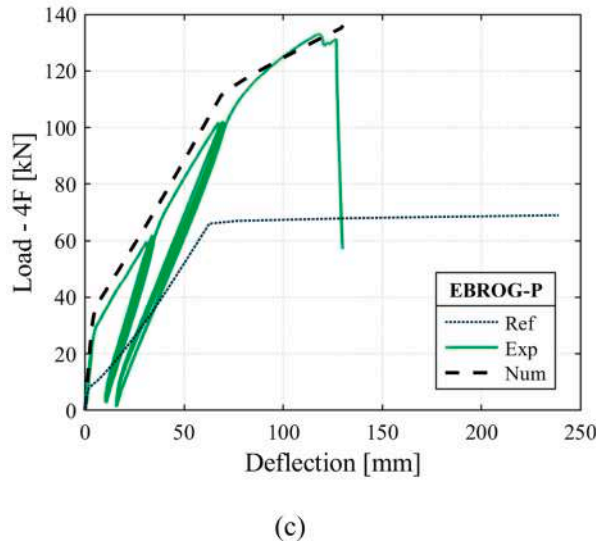

(c)

Fig. 17. Force vs. deflection at midspan: (a) EBR, (b) EBROG, c) EBROG-P.

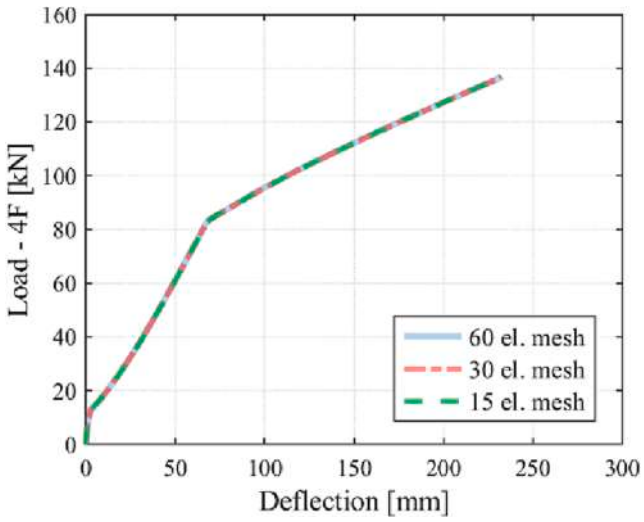

Fig. 18. Sensitivity analysis performed on the specimen EBROG.

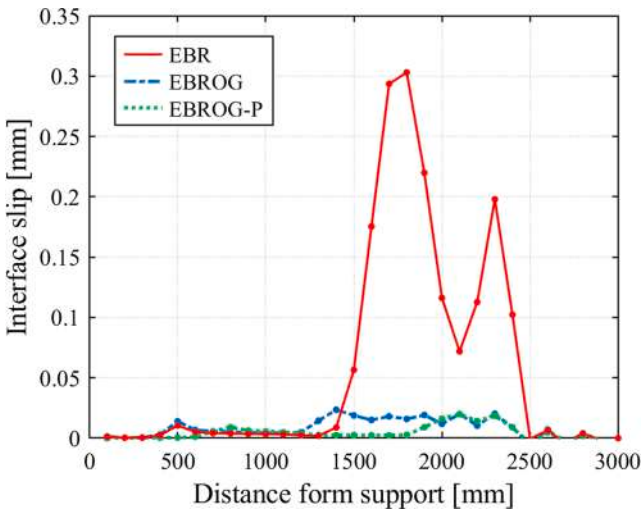

Fig. 19. Slip distribution under the failure load.

simulated for the same of completeness, although it was not tested. The comparison between the experimental results and the corresponding numerical simulation shows that there is very good agreement in terms of both shape of the overall force–deflection curve, and also in terms of predicted failure mode (debonding for EBR and FRP rupture in tension for EBROG systems). It is worth highlighting that all the main stages of the structural response (e.g. cracking, yielding and failure) are taken with more than reasonable accuracy, which not only corroborates the predicting potential of the numerical model, but also (and more importantly) it points out that the tested slab exhibit a mechanically intelligible behavior. A sensitivity analysis was performed on the EBROG specimen to understand whether the 30-element mesh discretization adopted in the present paper was capable to lead to sufficiently accurate results. The three graphs in Fig. 18 show that adopting meshes characterized by either 15 or 60 finite elements would lead to similar results. Therefore, the intermediate discretization (consisting of 30 beam elements each one 100 mm in length, as depicted in Fig. 14) was assumed in the present study.

Among other things, it emerges that the debonding failure of the externally bonded system can be predicted by the simple 2D beam-like FE model employed in this study (Fig. 14). The distributions of interface slips at ultimate, reported in Fig. 19, confirm that only in the case of the EBR slab intermediate debonding occurs, as the maximum slip (0.28

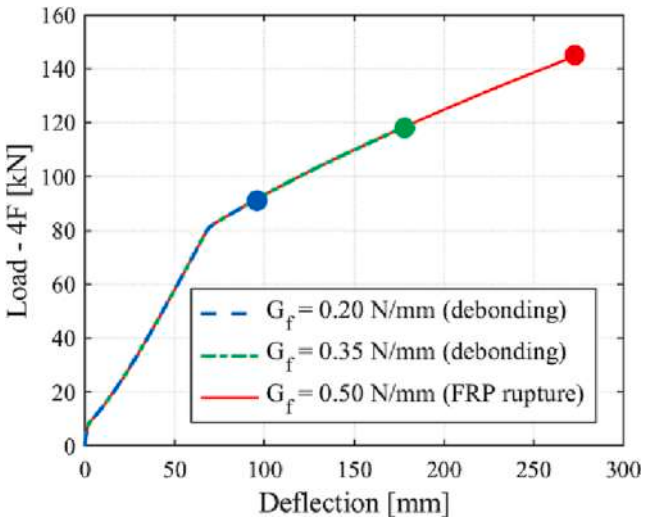

Fig. 20. Force vs. Deflection curves: EBR with variable fracture energy for the bond-slip law.

mm) overcomes the corresponding value assumed as a maximum value assumed in the bond-slip law (0.25 mm, according to Table 4).

However, it is worth highlighting that this result strongly depends on the value assumed for the fracture energy of the bilinear bond-slip curve represented in Fig. 16. In this respect, Fig. 20 for the EBR slab, shows how the post-yielding branch widens as higher values are assumed for fracture energy G_F, the failure mode turning from debonding (for low values of G_F) to tensile FRP rupture (for medium-to-high values of G_F).

A further comparison can be proposed in terms of relationship between the applied force (4F) and the resulting axial strain variation in the FRP strip at midspan (Fig. 21). The agreement between experimental measurements and numerical results is almost complete and confirms that the model can reproduce the overall response of the structural systems under consideration. The higher strain, as well as the higher ultimate load, predicted by the numerical model for the EBR slab-strip in comparison to the experiments (Fig. 17a), is justified by the chosen value of the interface fracture energy (G_F = 0.35 N/mm - Table 4) as elucidated above. The small difference in the ultimate strain in Fig. 17b and Fig. 17c is justified by the fact that the maximum experimental strain (Table 2) was slightly lower than the one provided for the numerical simulations. Due to the difficulties encountered in estimating the tensile strain in such testing conditions, as explained in the experimental section, the value of $\varepsilon_{f,u}$ for the numerical simulation was approximated to $1.4x10^4$ (Table 3).

Finally, as the numerical model has demonstrated remarkable accuracy in the points where the experimental measurements were available, it could be employed also to figure out how the structural response evolve in the points where no measurements were taken during the tests. In this regard, it was particularly interesting to scrutinize the evolution of the axial strains developed in the FRP strip throughout the loading process. For the sake of clarity, the focus was put on the three most significant stages of the structural response (once again, cracking, yielding and failure) for the three systems under consideration. Fig. 22 shows the continuous axial strain distribution in the FRP strip for the EBR RC slab calculated with the numerical model, the pointwise experimental values are represented by color markers. The occurrence of debonding results in maximum values of the axial strains that are significantly lower than the ultimate value assumed in the analyses ($\varepsilon_{f,u}$ = 14000 μm/m, as per Table 3). Because the experimental debonding occurred at an ultimate load of 100 kN, meanwhile the numerical model predicted a higher maximum force equal to 118 kN, both ultimate load steps are represented in figure.

Conversely, Fig. 23 shows that the axial strain at midspan under the

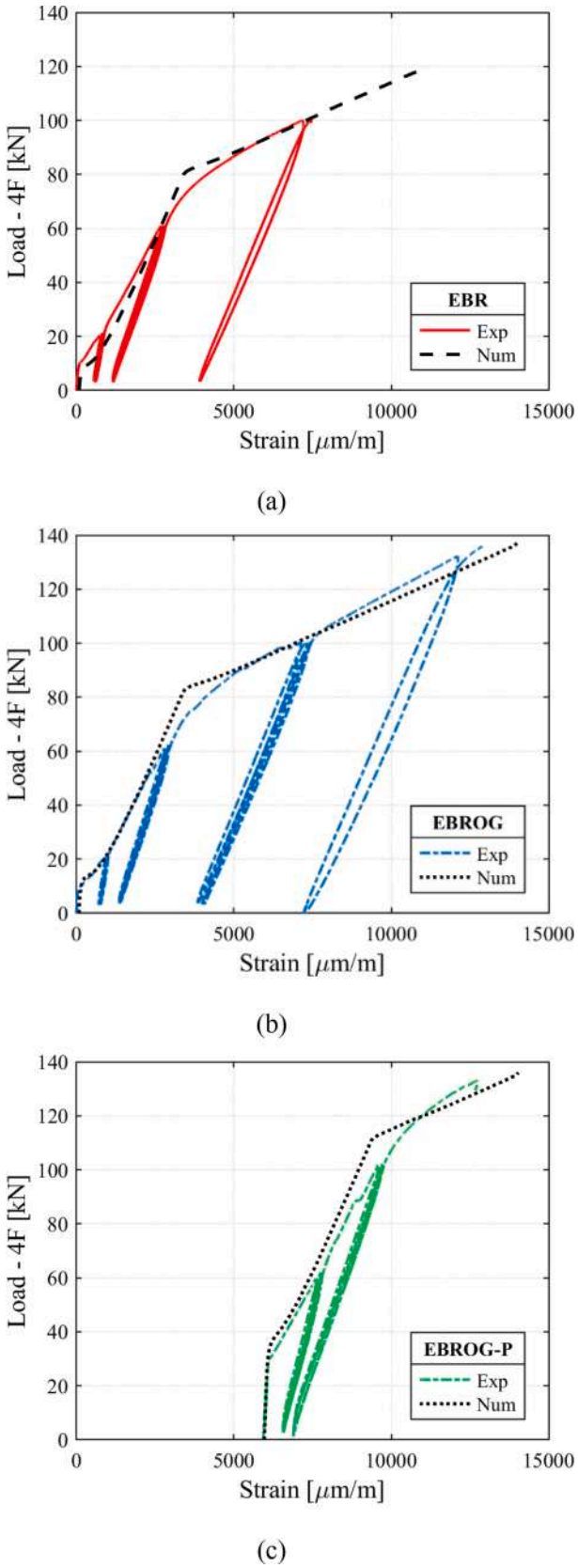

Fig. 21. Force vs. FRP axial strain at midspan: (a) EBR, (b) EBROG, c) EBROG-P.

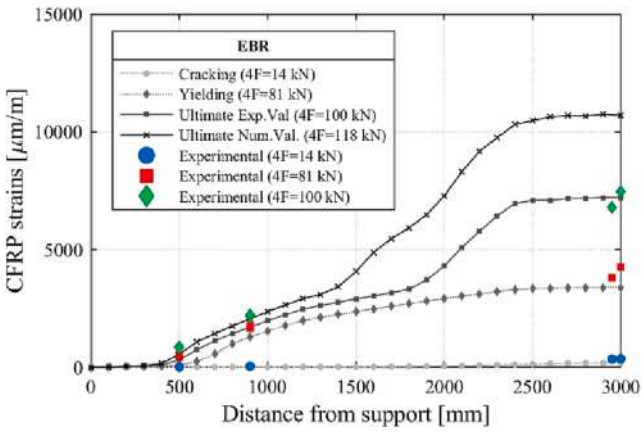

Fig. 22. Axial strain distribution throughout the CFRP (EBR slab).

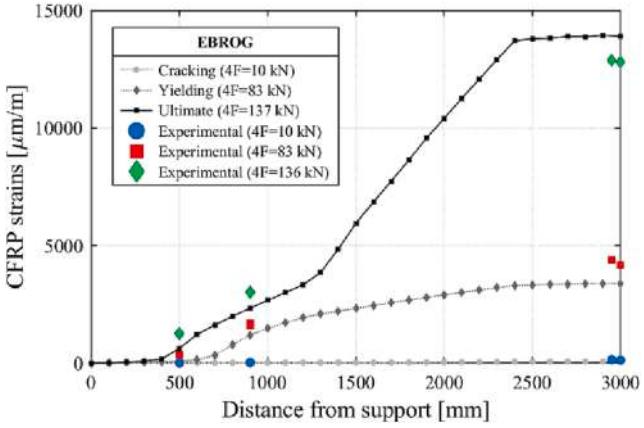

Fig. 23. Axial strain distribution throughout the CFRP (EBROG slab).

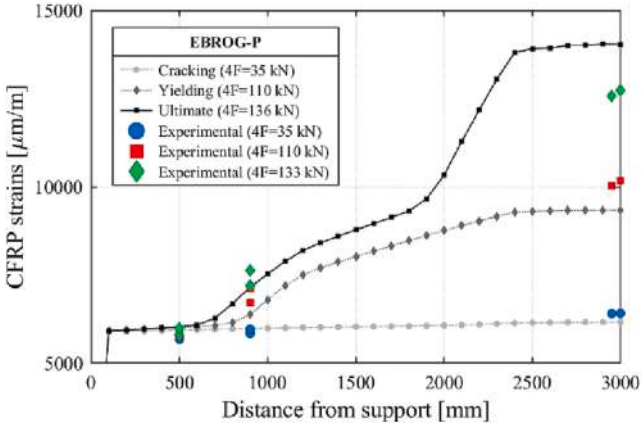

Fig. 24. Axial strain distribution throughout the CFRP (EBROG-P slab).

ultimate is equal to $\varepsilon_{f,u} = 14000$ μm/m, which confirms that the EBROG system can actually exploit the full potential of the FRP strip. Similar considerations can be pointed out from Fig. 24 for the EBROG-P system, as it attains the same midspan strain values of the EBROG one. Moreover, the effect of prestressing and the presence of the stirrups at the end of the FRP strips result in a value equal to $\varepsilon_{f,pre}$ at the end of the FRP strip.

5. Conclusions

The present paper reports the results of a large-scale experimental program intended at comparing the performance of RC slabs strengthened by either EBR or EBROG FRP strips, being the latter applied in either passive or pre-stressed state. The following main conclusions can be highlighted:

- the results of the large scale tests confirmed that EBROG system largely outperforms EBR one, as FRP strip debonding, which happened prematurely in the latter, was significantly delayed in the former;
- specifically, in RC members strengthened by both passive and pre-stressed EBROG strips, the axial strength of FRP was fully exploited and failure occurred due to fiber tearing at average axial strains very close to the ultimate value measured in tensile tests on the FRP strip;
- the failure load of the RC member strengthened with unstressed EBROG strips was 35%, the one with prestressed EBROG strips was 32% higher than the one with unstressed EBR strips, the corresponding strains in the strips incresed by 70%;
- the all-FRP anchorage system utilized for the pre-stressed EBROG strip demonstrated its effectiveness in avoiding premature end-anchorage failure after pre-stressing application and during the bending test;
- DIC monitoring allowed scrutinizing the evolution of the stress state developed in the tested slabs, as it clearly highlighted the effect of pre-stressing action on reducing flexural bending throughout the slab;
- the proposed numerical simulations demonstrated that the observed experimental behavior can be predicted on the bases of simple theoretical models, which makes the application of the tested techniques easier for design purposes.

Further studies, both experimental and theoretical in nature, are planned to further understand the influence of the groove shape and patterns on the resulting behavior of RC slabs with EBROG FRP strips.

CRediT authorship contribution statement

Niloufar Moshiri: Conceptualization, Methodology, Investigation, Writing – original draft, Formal analysis. **Enzo Martinelli:** Conceptualization, Methodology, Investigation, Writing – original draft, Funding acquisition, Formal analysis. **Matteo Breveglieri:** Writing – original draft, Visualization, Formal analysis. **Christoph Czaderski:** Resources, Writing – review & editing, Project administration, Funding acquisition.

Declaration of Competing Interest

The authors declare that they have no known competing financial interests or personal relationships that could have appeared to influence the work reported in this paper.

Data availability

Data will be made available on request.

Acknowledgments

The authors would like to thank Innosuisse - Swiss Innovation Agency (project 37516.1 IP-ENG) for the financial support, S&P Clever Reinforcement Company AG, Switzerland, for both their financial contributions and for providing material and technical assistance, and the Swiss National Science Foundation, which enabled Dr Enzo Martinelli to spend six months at the Laboratory of Structural Engineering of Empa, Dübendorf (CH), as part of the scientific exchange project IZSEZ0_202268/1. The technical team of the Laboratory of Structural

Engineering of the Empa, Switzerland, is gratefully acknowledged by the authors.

Appendix A. Supplementary data

Supplementary data to this article can be found online at https://doi.org/10.1016/j.engstruct.2023.116559.

References

[1] Meier U. Strengthening of structures using carbon fibre epoxy composites. Constr Build Mater 1995;9:341–51. https://doi.org/10.1016/0950-0618(95)00071-2.
[2] Ostrowski KA, Chastre C, Furtak K, Malazdrewicz S. Consideration of Critical Parameters for Improving the Efficiency of Concrete Structures Reinforced with FRP. Materials 2022;15:2774. https://doi.org/10.3390/ma15082774.
[3] Yang J, Haghani R, Blanksvärd T, Lundgren K. Experimental study of FRP-strengthened concrete beams with corroded reinforcement. Constr Build Mater 2021;301:124076. https://doi.org/10.1016/j.conbuildmat.2021.124076.
[4] Czaderski C, Meier U. EBR Strengthening Technique for Concrete, Long-Term Behaviour and Historical Survey. Polymers 2018;10(1):77. https://doi.org/10.3390/polym10010077.
[5] Burgoyne C. Fibre Reinforced Polymers – strengths, weaknesses, opportunities and threats. Proc of FRPRCS-9 Sydney. 2009.
[6] Teng JG, Chen JF. Mechanics of debonding in FRP-plated RC beams. Proc Inst Civ Eng: Struct 2009;162(5):335–45. https://doi.org/10.1680/stbu.2009.162.5.335.
[7] fib Externally applied FRP reinforcement for concrete structures-Technical report n.90. Fédération internationale du béton 2022. ISBN 978-2-88394-132-8.
[8] Teng JG, Chen GM, Chen JF. Effect of Load Distribution on IC Debonding in FRP-Plated RC Beams. In: Ye L, Feng P, Yue Q, editors. Advances in FRP Composites in Civil Engineering. Berlin, Heidelberg: Springer Berlin Heidelberg; 2011. p. 485–9.
[9] Bilotta A, Faella C, Martinelli E, Nigro E. Design by testing procedure for intermediate debonding in EBR FRP strengthened RC beams. Eng Struct 2013;46:147–54. https://doi.org/10.1016/j.engstruct.2012.06.031.
[10] Breveglieri, M., Hosseini, A., Czaderski, C. FRP-to-concrete debonding - global and local bond behavior. In Proc. of CICE 2018 - Paris, 353-360.
[11] Zhang J, Guo R, Li S, Zhao S. Prediction of the IC debonding failure of FRP-strengthened RC beams based on the cohesive zone model. Lat Am J Solids Struct 2020;17(6). https://doi.org/10.1590/1679-78256208.
[12] Li P, Zhao Y, Wu Y, Lin J. Effect of defects in adhesive layer on the interfacial bond behaviors of externally bonded CFRP-to-concrete joints. Eng Struct 2023;278:115495. https://doi.org/10.1016/j.engstruct.2022.115495.
[13] Li P, Zeng J, Li W, Zhao Y. Effect of concrete heterogeneity on interfacial bond behavior of externally bonded FRP-to-concrete joints. Constr Build Mater 2022;359:239483. https://doi.org/10.1016/j.conbuildmat.2022.129483.
[14] Napoli A, Matta F, Martinelli E, Nanni A, Realfonzo R. Modelling and verification of response of RC slabs strengthened in flexure with mechanically fastened FRP laminates. Mag Concr Res 2010;62(8):593–605.
[15] Napoli A, Bank LC, Brown VL, Martinelli E, Matta F, Realfonzo R. Analysis and design of RC structures strengthened with mechanically fastened FRP laminates: A review. Compos B: Eng 2013;55:386–99. https://doi.org/10.1016/j.compositesb.2013.06.038.
[16] Sena Cruz JM, Barros J. Bond between near-surface mounted carbon-fiber-reinforced polymer laminate strips and concrete. J Compos Constr 2004;8(6):519–27. https://doi.org/10.1061/(ASCE)1090-0268(2004)8:6(519).
[17] Karayannis GC, Golias E. Full-scale experimental testing of RC beam-column joints strengthened using CFRP ropes as external reinforcement. Eng Stuct 2022;250:113305. https://doi.org/10.1016/j.engstruct.2021.113305.
[18] Mostofinejad D, Mahmoudabadi E. Grooving as Alternative Method of Surface Preparation to Postpone Debonding of FRP Laminates in Concrete Beams. J Compos Constr 2010;14(6):804–11. https://doi.org/10.1061/(ASCE)CC.1943-5614.0000117.
[19] Mostofinejad D, Shameli SM, Hosseini A. EBROG and EBRIG methods for strengthening of RC beams by FRP sheets. Eur J Environ Civ 2014;18(6):652–68. https://doi.org/10.1080/19648189.2014.900523.
[20] Sanginabadi K, Yazdani A, Mostofinejad D, Czaderski C. Bond behavior of FRP composites attached to concrete using EBROG method: A state-of-the-art review. Compos Struct 2022;299:116060. https://doi.org/10.1016/j.compstruct.2022.116060.
[21] Hosseini A, Mostofinejad D. Effect of groove characteristics on CFRP-to-concrete bond behavior of EBROG joints: Experimental study using particle image velocimetry (PIV). Constr Build Mater 2013;49:364–73. https://doi.org/10.1016/j.conbuildmat.2013.08.036.
[22] Moshiri N, Tajmir-Riahi A, Mostofinejad D, Czaderski C, Motavalli M. Experimental and analytical study on CFRP strips-to-concrete bonded joints using EBROG method. Compos B: Eng 2019;158:437–47. https://doi.org/10.1016/j.compositesb.2018.09.046.
[23] Tajmir-Riahi A, Moshiri N, Mostofinejad D. Bond mechanism of EBROG method using a single groove to attach CFRP sheets on concrete. Constr Build Mater 2019;197:693–704.
[24] Tajmir-Riahi A, Moshiri N, Czaderski C, Mostofinejad D. Effect of the EBROG method on strip-to-concrete bond behavior. Constr Build Mater 2019;220:701–71. https://doi.org/10.1016/j.conbuildmat.2019.06.065.
[25] Moshiri N., Martinelli E., Czaderski C. Bond Mechanism of non-prestressed and prestressed CFRP to Concrete with EBR and EBROG methods. Proc of Bond in Concrete 2022 – Stuttgart.
[26] Mofrad MH, Mostofinejad D, Hosseinib A. A generic non-linear bond-slip model for CFRP composites bonded to concrete substrate using EBR and EBROG techniques. Compos Struct 2019;220:31–44. https://doi.org/10.1016/j.compstruct.2019.03.063.
[27] Moshiri N, Czaderski C, Mostofinejad D, Motavalli M. Bond resistance of prestressed CFRP strips attached to concrete by using EBR and EBROG strengthening methods. Constr Build Mater 2012:266–121209. https://doi.org/10.1016/j.conbuildmat.2020.121209.
[28] Czaderski C. Strengthening of reinforced concrete members by prestressed, externally bonded reinforcement with gradient anchorage. ETH Zürich; 2012. p. 458. Dr. Thesis,.
[29] Moshiri N, Martinelli E, Czaderski C, Mostofinejad D, Hosseini A, Motavalli M. Bond behavior of prestressed cfrp strips to concrete using ebrog method – experimental and analytical evaluation. J Compos Constr 2022. https://doi.org/10.1061/JCCOF2/CCENG-3851.
[30] Moshiri N, Czaderski C, Mostofinejad D, Hosseini A, Sanginabadi K, Breveglieri M, et al. Flexural strengthening of RC slabs with nonprestressed and prestressed CFRP strips using EBROG method. Compos B: Eng 2020;201:108359. https://doi.org/10.1016/j.compositesb.2020.108359.
[31] Hüppi M., Hosseini A., Moshiri N., Mostofinejad D., C Czaderski C., Motavalli M. Method for strengthening concrete or timber structures using CFRP strips and concrete or timber structures strengthened by this method. US Patent 11,299,895.
[32] Michels J, Martinelli E, Czaderski C, Motavalli M. Prestressed CFRP strips with gradient anchorage for structural concrete retrofitting: Experiments and numerical modeling. Polymers 2014;6(1):114–31. https://doi.org/10.3390/polym6010114.
[33] Breveglieri M, Czaderski C, Michels J. The Gradient Anchorage Method for Prestressed CFRP Strips: from the Development to the Strengthening of an 18 M Long Bridge Girder. SJCE 2018;26(3):29–40. https://doi.org/10.2478/sjce-2018-0018.
[34] Faella C, Martinelli E, Nigro E. Formulation and validation of a theoretical model for intermediate debonding in FRP-strengthened RC beams. Compos B: Eng 2008;39(4):645–55.
[35] Martinelli E, Faella C, di Palma G. Shear-Flexible Steel-Concrete Composite Beams in Partial Interaction: Closed-Form "Exact" Expression of the Stiffness Matrix. J Eng Mech 2012;138(2):151–63.
[36] Martinelli E. A general numerical model for simulating the long-term response of two-layer composite systems in partial interaction. Compos Struct 2021;257(112929).
[37] Matlab. version 9.9.0 (R2020b). Natick, Massachusetts: The MathWorks Inc; 2020.
[38] Sargin M. Stress-Strain Relationship for Concrete and the Analysis of Structural Concrete Sections. Study: University of Waterloo; 1971.
[39] S&P Clever Reinforcement Company AG. S&P HP Resin 220 Epoxy Adhesive-technical data sheet. Ver. 01.2021.
[40] Correlated Solutions Inc. - Vic-3d software manual. version 8.4.
[41] CEN. Eurocode 2: Design of concrete structures - Part 1-1: General rules and rules for buildings 2004.